# Forest degradation contributes more to carbon loss than forest cover loss in North American boreal forests

Ling Yu, Lei Fan, Philippe Ciais, Jingfeng Xiao, Frédéric Frappart, Stephen Sitch, Jingming Chen, Xiangming Xiao, Rasmus Fensholt, Zhongbing Chang, et al.

International Journal of Applied Earth Observation and Geoinformation 128 (2024) 103729

Contents lists available at ScienceDirect

International Journal of Applied Earth Observation and Geoinformation

journal homepage: www.elsevier.com/locate/jag

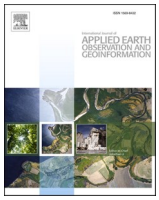

# Forest degradation contributes more to carbon loss than forest cover loss in North American boreal forests

Ling Yu [a,b], Lei Fan [a,b,*], Philippe Ciais [c], Jingfeng Xiao [d], Frédéric Frappart [e], Stephen Sitch [f], Jingming Chen [g], Xiangming Xiao [h], Rasmus Fensholt [i], Zhongbing Chang [j], Hongqian Fang [a,b], Xiaojun Li [e], Tiangxiang Cui [k], Mingguo Ma [a,b], Jean-Pierre Wigneron [e]

[a] Chongqing Jinfo Mountain Karst Ecosystem National Observation and Research Station, School of Geographical Sciences, Southwest University, Chongqing 400715, China
[b] Chongqing Engineering Research Center for Remote Sensing Big Data Application, School of Geographical Sciences, Southwest University, Chongqing 400715, China
[c] Laboratoire des Sciences du Climat et de l'Environnement, LSCE/IPSL, CEA-CNRS-UVSQ, Université Paris Saclay, Gif-sur-Yvette 91191, France
[d] Earth Systems Research Center, Institute for the Study of Earth, Oceans, and Space, University of New Hampshire, Durham, NH 03824, USA
[e] ISPA, UMR 1391, INRAE Nouvelle-Aquitaine, Université de Bordeaux, Villenave d'Ornon F-33140, France
[f] College of Life and Environmental Sciences, University of Exeter, Exeter EX4 4RJ, UK
[g] Department of Geography, University of Toronto, Toronto ON M5S 3G3, Canada
[h] Department of Microbiology and Plant Biology, Center for Earth Observation and Modeling, University of Oklahoma, Norman OK 73019, USA
[i] Department of Geosciences and Natural Resource Management, University of Copenhagen, Copenhagen 1350, Denmark
[j] Key Laboratory of Natural Resources Monitoring in Tropical and Subtropical Area of South China, Surveying and Mapping Institute Lands and Resource Department of Guangdong Province, Guangzhou 510663, China
[k] Co-Innovation Center for Sustainable Forestry in Southern China, Nanjing Forestry University, Nanjing, Jiangsu 210042, China

ARTICLE INFO

*Keywords:*
Canadian boreal forests
Carbon balance
Remote sensing
Forest degradation

ABSTRACT

The carbon sinks of North American boreal forests have been threatened by global warming and forest disturbances in recent decades, but knowledge about the carbon balance of these forests in recent years remains unknown. We tracked annual aboveground carbon (AGC) changes from 2016 to 2021 across the forest regions of NASA's Arctic Boreal Vulnerability Experiment (ABoVE) core study domain, using Vegetation Optical Depth derived from low-frequency passive microwave observations. The results showed that these forests showed a net AGC increase of + 28.49 Tg C/yr during the study period, with total AGC gains of + 219.34 Tg C/yr counteracting total AGC losses of −190.86 Tg C/yr. Forest degradation (-162.21 Tg C/yr), defined as a reduction in the capacity of forest to provide goods and services, contributes 5 times more to the total AGC loss than forest cover loss (-28.65 Tg C/yr), defined as the complete removal of tree cover. This indicates that degradation has dominated AGC loss in the region.

## 1. Introduction

North American boreal forests have attracted particular attention due to their critical role in regulating the global carbon budget (Gauthier et al., 2015). Global warming, forest disturbances and degradation have significant negative impacts on the carbon budget of these forests (Kurz et al., 2008b). Yet, global warming may also have the potential to increase the productivity of these forests (Wang et al., 2023). Thus, whether North American boreal forests have acted as a carbon sink or carbon source in recent years remains uncertain.

In recent decades, a large variation in carbon estimates has been noted in North American boreal forests: +50 Tg C/yr using ecosystem models (positive values represent a net carbon sink) (Stinson et al., 2011); −53 Tg C/yr using forest inventories (Pan et al., 2011); +14 Tg C/yr using optical remote sensing data (Wang et al., 2021); and −6 Tg C/yr using high-frequency passive microwave remote sensing data (Liu et al., 2015). These discrepancies in carbon estimates have resulted in a limited comprehension of the carbon budget in North American boreal forests.

The carbon budget of North American boreal forests is threatened by

* Corresponding author at: Chongqing Jinfo Mountain Karst Ecosystem National Observation and Research Station, School of Geographical Sciences, Southwest University, Chongqing 400715, China.
*E-mail address:* leifan33@swu.edu.cn (L. Fan).

https://doi.org/10.1016/j.jag.2024.103729
Received 13 September 2023; Received in revised form 11 February 2024; Accepted 18 February 2024
Available online 6 March 2024

forest cover loss and degradation (Kurz, 2010). Forest cover loss, such as stand-replacing fires, clear-cutting and severe insect outbreaks, results in the elimination of living aboveground biomass and photosynthetically sequestered carbon from the atmosphere (Hansen et al., 2013). During 2000–2012, the carbon loss caused by forest cover loss in western North American boreal forests was 22.3 Tg C/yr (Yu et al., 2023). Forest degradation leads to carbon loss without completely removing the living aboveground biomass, including partial mortality from non-stand-replacing disturbances (e.g., wildfires, selective logging and droughts) (Gao et al., 2020). In recent decades, non-stand-replacing insect outbreaks were estimated to have caused a carbon loss of 13.5 Tg C/yr in Canada (Kurz et al., 2008a). However, due to challenges in separating forest degradation from forest cover loss, most studies on forest carbon loss tend to focus primarily on either forest cover loss or degradation. Thus, the relative contributions of forest cover loss and degradation to carbon loss in North American boreal forests remain unknown.

Previous studies showed that the forest carbon sink is affected by forest age and tree species (Gao et al., 2016; Rogers et al., 2015). Forest age affects light-use efficiency and the capacity of biomass accumulation in forests (Besnard et al., 2018). A previous study revealed that the maximum carbon sink occurs primarily in forests aged 30–120 years, and the carbon sink of forests older than 120 years is generally reduced (Pregitzer and Euskirchen, 2004). In addition, diverse tree species exhibit unique capacities to withstand disturbances, which can significantly impact the carbon sink in forests (Hermosilla et al., 2022). For instance, pine species are prone to infestation by the mountain pine beetle (Kurz et al., 2008a) and aspen species are vulnerable to high intensity crown fires (Shinneman et al., 2013). Therefore, exploring the carbon changes of different forest ages and tree species is vital for gaining insight into the carbon dynamics of North American boreal forests.

Previous estimates of the carbon dynamics of North American boreal forests relied primarily on forest inventory data (Stinson et al., 2011), atmospheric $CO_2$ observations inversion models (Hayes et al., 2012), and satellite optical data (Wang et al., 2021). Yet, estimates from inventory data and atmospheric inversion models can exhibit high uncertainty due to sparse observation networks and uncertainties in the inversion models (Gurney et al., 2004). Using optical remote sensing data to infer biomass changes can be hindered by clouds, aerosols, and saturation effects in areas with dense vegetation (Myers-Smith et al., 2020). High-frequency passive microwave remote sensing data are least affected by atmospheric and cloud influences, but tend to saturate in forested regions and are generally regarded as unsuitable for accurate biomass carbon monitoring (Brandt et al., 2018a). The Global Ecosystem Dynamics Investigation (GEDI) data are highly promising for aboveground carbon (AGC) estimation (Xiao et al., 2019). However, the limited coverage between 51°N and 51°S latitudes restricts its application in estimating AGC for North American boreal forests, and inferring AGC changes requires models to combine GEDI data with time series from other instruments (Dubayah et al., 2020; Shendryk, 2022).

The low-frequency Vegetation Optical Depth data at L-band (1.4 GHz) (L-VOD), retrieved from passive microwave satellite observation, exhibits high sensitivity to vegetation aboveground biomass and does not saturate in dense forests (Frappart et al., 2020; Li et al., 2022; Fan et al., 2022). This makes it a good alternative for estimations of aboveground biomass (Yang et al., 2023). The availability of L-VOD data for multiple years allows us to accurately estimate aboveground biomass in North American forests, and thereby infer AGC change over time.

In this study, L-VOD products were used to estimate AGC stocks and changes over the western North American boreal forests for 2016–2021. The aims were to: (1) represent the spatial patterns of AGC, (2) investigate AGC dynamics from 2016 to 2021, related to forest ecoregions, forest age and tree species, and (3) quantify AGC loss caused by forest cover loss and degradation.

## 2. Materials

### 2.1. The study region

The forest regions within NASA's Arctic Boreal Vulnerability Experiment (ABoVE) core study domain, spanning from 100°W to 168°W and 52°N to 74°N and encompassing the western provinces of Canada and the state of Alaska in the USA (Loboda et al., 2019), were selected as the study region (Fig. 1). Based on the Environmental Protection Agency's (EPA) Level 2 Ecoregions for North America (Omernik and Griffith, 2014), the study region was divided into eight eco-regions, including the Alaska boreal interior, the Western cordillera, the Taiga cordillera, the Taiga plain, the Softwood shield, the Taiga shield, the Boreal cordillera and the Boreal plain eco-regions (Fig. 1). Eco-regions such as the Marine West Coast Forest, the Tundra and the Temperate Prairies that had limited overlap with the study region were excluded.

### 2.2. Land cover map

We used the CCI land cover map in 2016 (Defourny et al., 2017) to identify forest regions (Fig. 1). The spatial resolution of this map (300 m) was aggregated to 0.25 degree using the majority rule. This involved recording the land cover type that had the largest number of 300 m native spatial resolution pixels within each 0.25 degree pixel. The aggregated 0.25 degree CCI land cover map contains forest, shrubland, grassland, sparse vegetation, cropland, bare area, and water (Table S1). Non-forest land cover types were masked as we mainly focused on AGC dynamics in forest regions.

### 2.3. Aboveground biomass benchmark map

The updated version of Saatchi et al. (2011) aboveground biomass (AGB) benchmark map, which is a static AGB map of global forests with 1 km spatial resolution in 2015, was used to calibrate L-VOD. This updated map was produced by combining the satellite datasets from the Shuttle Radar Topography Mission (SRTM) with Landsat data and Advanced Land Observing Satellite (ALOS) data (Carreiras et al., 2017). The original unit of this AGB density data was Mg/ha, which we converted to AGC density (Mg C/ha) by multiplying it by a factor of 0.5 (Brandt et al., 2018b). This map was aggregated to 0.25 degree by using a simple averaging method.

### 2.4. L-VOD

The SMOS-SMAP-INRAE-BORDEAUX L-VOD Version 1 product (SMOSSMAP-IB, V1) (Li et al., 2022), derived from the Soil Moisture and Ocean Salinity (SMOS) and the Soil Moisture Active Passive (SMAP) satellites, was used to estimate AGC changes. This SMOSSMAP-IB product provides global-scale daily L-VOD data with 0.25 degree spatial resolution from 1 April 2015 to 31 December 2021. The SMAP-IB retrieval algorithm, a mono-angular retrieval algorithm, was used to retrieve these L-VOD data (Li et al., 2022; Wigneron et al., 2007). In this retrieval algorithm, the merged brightness temperature observations from both the SMOS and SMAP sensors were used as input data (Li et al., 2022). The study period was from 2016 to 2021, which was limited by the short coverage time of the SMOSSMAP-IB product.

To restrict the study to the best quality data, the daily L-VOD pixels associated with frozen conditions, water bodies and strong topography were excluded. We produced monthly L-VOD by calculating the mean of all high-quality daily L-VOD data within each month. Considering that VOD data are often affected by frozen and snowy conditions, the yearly L-VOD was calculated as the average of the monthly L-VOD from June to September in a year.

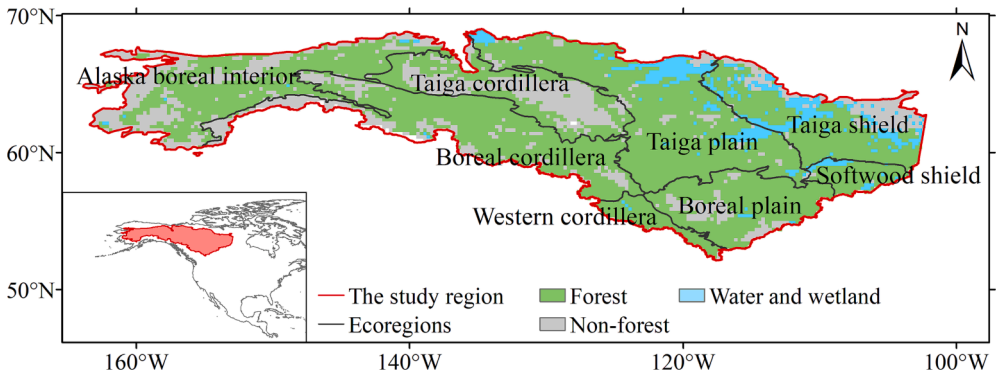


**Fig. 1.** The distribution of forest regions and the EPS's Level 2 Eco-regions. The background shows the forest regions that were obtained from the European Space Agency's Climate Change Initiative (CCI) for the year 2016.

### 2.5. Forest age data

The forest age data across Canada provides a distribution of forest age with 30 m resolution circa 2019 (Maltman et al., 2023). This map was generated from Landsat and MODIS remote sensing data. The methods employed to determine forest age included the 'disturbance approach', 'recovery approach' and 'allometric approach'. Using a simple average method, this forest age map was aggregated to 0.25 degree spatial resolution. The aggregated map encompasses forest age spans from 10 to 130 years and was divided into six 20-year age class bins: 10–30, 30–50, 50–70, 70–90, 90–110, >110 years (Figure S1).

### 2.6. Tree species data

The tree species data was obtained from Hermosilla et al. (2022). 37 tree species were mapped at 30 m resolution in this map, representing the conditions of 2019. This dataset was produced by integrating Canada's national forest inventory data, spectral information derived from Landsat imagery and ancillary information (e.g., climate data, elevation data, and phenology data) using the Random Forests machine learning algorithm. The tree species map was aggregated to 0.25 degree spatial resolution using the majority rule, which involves recording the tree species with the largest number of 30 m native spatial resolution pixels within each 0.25 degree pixel. There are 10 tree species in this aggregated map (i.e., Subalpine fir, White birch, Tamarack, Engelmann spruce, White spruce, Black spruce, Jack pine, Lodgepole pine, Balsam poplar, Trembling aspen). We categorized the species based on their genus (i.e., Engelmann spruce, White spruce, and Black spruce were grouped as spruce, Jack pine and Lodgepole pine were grouped as pine). Also, we calculated the area fraction of each tree species within the study region, and the tree species with an area fraction less than 1 % (i.e., White birch, Tamarack and Balsam poplar) were excluded. The 0.25 degree tree species map used in this study included four tree species: spruce, fir, pine and aspen (Figure S2).

### 2.7. Forest cover loss data

The forest cover loss data (version 1.9) was obtained from Hansen et al. (2013), providing annual forest cover loss from 2000 to 2021 at 30 m resolution. Forest cover loss refers to the transition from forest to non-forest. The "lossyear" layer of this dataset records the year when forest cover loss occurred, representing the loss of forest detected during 2000–2021. The forest cover loss data for 2016–2021 used in this study was aggregated to 0.25 degree by summing the forest cover loss area within each L-VOD grid cell.

### 2.8. Active fire dataset

The active fire data originated from MOD14A2 (Version 061) (Giglio et al., 2016). This dataset is an eight-day composite fire-mask at 1 km resolution. According to the quality layer included in each MOD14A2 file, pixels with nominal and high confidence were selected as the mask to identify the good-quality active fire observations. The forest cover loss data for 2016–2021 used in this study were aggregated to 0.25 degree resolution using the summing method, which refers to sum up the forest cover loss area within each 0.25 degree pixel.

### 2.9. Stand-replacing fire

We used the MOD14A2 active fire data and the forest cover loss data from Hansen et al. (2013) to identify stand-replacing fires. First, the forest cover loss map (30 m) was aggregated to 1 km by recording the dominant year of forest cover loss within each MOD14A2 active fire grid cell. Second, the MOD14A2 active fire data was overlapped with the forest cover loss map for each year from 2016 to 2021 at 1 km spatial resolution to identify the yearly stand-replacing fire pixels. At last, the stand-replacing fire pixels from 2016 to 2021 were aggregated to 0.25 degree by calculating the sum area of stand-replacing fires within each L-VOD grid cell.

## 3. Methods

### 3.1. L-VOD derived annual AGC dynamics

Annual AGC was calculated from L-VOD using the method proposed by Liu et al. (2015) and Fan et al. (2019). The four-parameter function was used to calibrate the relationship between L-VOD and AGC:

$$AGC = a \times \frac{\arctan(b \times (VOD - c)) - \arctan(-b \times c)}{\arctan(b \times (Inf - c)) - \arctan(-b \times c))} + d \quad (1)$$

where a, b, c and d are the fitted coefficients, Inf was set to $10^{10}$. We used the Saatchi AGC benchmark map and L-VOD in 2016 to calibrate Eq. (1). Using Eq. (1), yearly L-VOD from 2016 to 2021 was converted into yearly AGC density (Mg C/ha). The AGC stock was then calculated by multiplying the AGC density by the area of the corresponding pixel. The year used for calibration proved to have little impact on the calibrated curves. The calibrated relationships between L-VOD from 2016 to 2021 and the Saatchi AGC benchmark map were calculated, showing very similar correlations (r: 0.71–0.73) from 2016 to 2021 (Figure S3).

We conducted a bootstrap cross-validation (sampling rate = 80 %, iterations = 1000) method to evaluate the calibration errors for the year 2016 (Fan et al., 2019). The cross-validation results showed high correlation values (r = 0.75) and low root mean square difference values (RMSE = 0.04 Pg C) between the benchmark AGC map and the bootstrapped AGC estimates (Table S2), suggesting that errors caused by sampling and calibration are limited. Furthermore, the retrieved AGC displays a small 95 % bootstrap confidence interval, suggesting limited

errors stemming from the process of sampling and calibration (Table S2).

To quantify the accuracy of the AGC derived from L-VOD, we compared the L-VOD AGC with the Saatchi AGC benchmark map. A high correlation value ($r = 0.74$) was achieved when comparing the estimated AGC with the Saatchi AGC benchmark map (Figure S4). Furthermore, in order to conduct the temporal validation, we used multi-year AGC maps from CCI to validate the AGC changes derived from L-VOD for 2017–2020 (Zhao et al., 2023). A significant correlation ($r = 0.86$, $p < 0.01$) was observed between the AGC changes derived from L-VOD and those obtained from CCI data (Figure S5), and the grid cells with lower uncertainty of AGC changes in the CCI data (lighter color in Figure S5) are closer to the 1:1 line.

### 3.2. AGC loss caused by forest cover loss and degradation

Forest cover loss and degradation dominate the total AGC loss in a grid cell (Fan et al., 2022). All mechanisms that do not result in forest cover loss were defined as forest degradation in this study. To conduct a simple estimate of the AGC loss resulting from forest cover loss and degradation, the method introduced by Harris et al. (2012) and Qin et al. (2021) was adopted in this study. First, the total AGC loss ($AGC_{totalloss}$) at 0.25 degree spatial resolution was calculated using Eq. (2). Second, the AGC loss caused by forest cover loss ($AGC_{forestcoverloss}$) was computed by multiplying the total area of forest cover loss during 2017–2021 ($Arealoss_{total}$) by the AGC density in 2016 ($AGCdensity_{2016}$) using Eq. (3). The total area of forest cover loss ($Arealoss_{total}$) was computed by summing the forest loss area from 2017 to 2021 at 0.25 degree resolution using the Hansen et al. (2013) forest cover loss data. Third, we calculated the difference between the total AGC loss ($AGC_{totalloss}$) and the AGC loss from forest cover loss ($AGC_{forestcoverloss}$) as the AGC loss from degradation ($AGC_{degradation}$), as shown in Eq. (4).

$$AGC_{totalloss} = \sum (AGC_{i+1} - AGC_i), \text{ with } (AGC_{i+1} - AGC_i < 0) \quad (2)$$

$$AGC_{forestcoverloss} = \sum (Arealoss_{total} \times AGCdensity_{2016}) \quad (3)$$

$$AGC_{degradation} = AGC_{totalloss} - AGC_{forestcoverloss} \quad (4)$$

where $i$ represents the year from 2016 to 2020.

The total AGC loss cause by forest cover loss was subsequently divided into components stemming from stand-replacing fires and other stand-replacing processes (e.g., clear-cutting, severe insect outbreaks, and drought) (Fan et al., 2022). The AGC loss from stand-replacing fires ($AGC_{fire}$) was calculated by multiplying the gross area of stand-replacing fire during 2017–2021 ($Arealoss_{fire}$) by the AGC density in 2016 ($AGCdensity_{2016}$) using Eq. (5), in which $Arealoss_{fire}$ was calculated as the sum of stand-replacing fire area from 2017 to 2021 over each 0.25 degree resolution pixel. At last, the AGC loss from other stand-replacing processes ($AGC_{others}$) was computed as the difference of the AGC loss from forest cover loss ($AGC_{forestcoverloss}$) and the AGC loss from stand-replacing fires ($AGC_{fire}$) using Eq. (6) (Fan et al., 2022).

$$AGC_{fire} = \sum (Arealoss_{fire} \times AGCdensity_{2016}) \quad (5)$$

$$AGC_{others} = AGC_{forestcoverloss} - AGC_{fire} \quad (6)$$

### 3.3. Statistical analysis

To analyze the spatial patterns of AGC density, we calculated variations in AGC density based on forest age, eco-region, and tree species. A one-way analysis of variance (ANOVA) method was employed to test for significant differences ($p < 0.05$) in AGC density among different forest ages, eco-regions, and tree species. In addition, we used the standard deviation to represent the uncertainties of AGC change for different forest ages and tree species, which was calculated based on the bootstrap cross-validation method (sampling rate = 80 %, iterations = 1000).

## 4. Results

### 4.1. Spatial patterns of AGC

Over the study period (2016–2021), the average AGC density derived from L-VOD across the study region was 23.72 Mg C/ha (Fig. 2a). AGC density varied substantially by latitude, forest age, eco-region, and tree species. The AGC density exhibited a decreasing trend as latitude increased from 52°N to 70°N (Fig. 2a, Fig. 2b). The highest AGC density was found around 52°N (34.37 Mg C/ha), and the lowest AGC density was mainly distributed around 70°N (11.93 Mg C/ha) (Fig. 2b). These results suggest that there is a large latitudinal gradient in the distribution of AGC density.

AGC density increased with increasing forest age across the six forest age classes averaged over the 0.25 degree pixels (Fig. 3a). The highest AGC density, reaching 31.39 Mg C/ha, was observed in forests aged 90–110 years old, for then to level out in forests that were older than 110 years old (Fig. 3a). The lowest AGC density was observed in forests aged 10–30 years old at 10.89 Mg C/ha (Fig. 3a).

In terms of tree species, fir had the largest AGC density (34.50 Mg C/ha), followed by aspen (26.11 Mg C/ha) and pine (25.68 Mg C/ha), while spruce showed the lowest AGC density (22.02 Mg C/ha) (Fig. 3b). Regarding eco-regions, the Western cordillera eco-region had the largest AGC density (38.45 Mg C/ha) (Fig. 3c), while the Softwood shield eco-region had the lowest AGC density (8.28 Mg C/ha) (Fig. 3c).

### 4.2. AGC dynamics from 2016 to 2021

AGC estimates for Western North American boreal forests using L-VOD showed a net increase of 28.49 Tg C/yr from 2016 to 2021 in the study region (Fig. 4a). This net AGC increase reflects a balance between total AGC gains of + 219.34 Tg C/yr and total AGC losses of −190.86 Tg C/yr (Table S3). With regard to the spatial pattern of AGC change, a widespread net increase was observed over 63 % of the study region (Fig. 4b). The most pronounced net AGC increase was observed in the Boreal cordillera and the Alaska boreal interior eco-regions (Fig. 4b). About 37 % of the study region exhibited a net AGC decrease, primarily in the Taiga plain and the Boreal plain eco-regions (Fig. 4b).

In terms of eco-region, the Boreal cordillera eco-region showed the largest AGC increase (+18.09 Tg C/yr) (Fig. 5g), followed by the Alaska boreal interior eco-region (+13.17 Tg C/yr) (Fig. 5a). In contrast, the Taiga plain eco-region and the Boreal plain eco-region showed a net AGC decline of −4.44 Tg C/yr (Fig. 5c) and −3.05 Tg C/yr (Fig. 5f), respectively. The Taiga cordillera eco-region and the Western cordillera eco-region had a net AGC increase of + 3.44 Tg C/yr and + 1.19 Tg C/yr, respectively (Fig. 5b, Fig. 5h). The Taiga shield eco-region and the Softwood shield eco-region had a nearly neutral AGC balance (Fig. 5d,

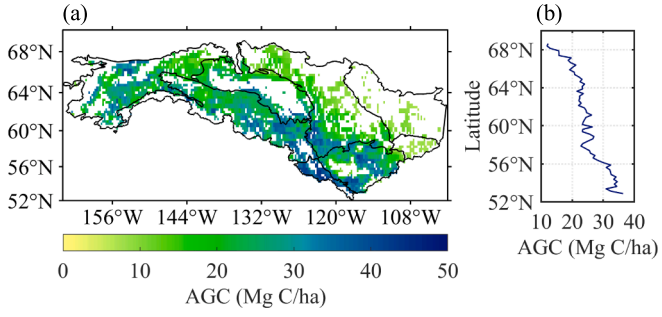


**Fig. 2.** Spatial distribution of AGC density based on L-VOD. (a) Averaged AGC density for the period from 2016 to 2021. (b) Variation of AGC density with latitude.

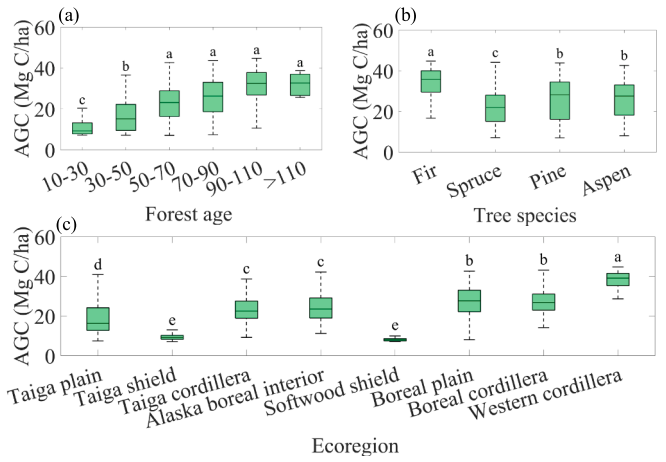


**Fig. 3.** Variations in AGC density across forest ages (a), tree species (b) and eco-regions (c). a ~ e in each sub-figure shows whether there is a significant difference ($p < 0.05$) in AGC density between forest age, tree species and ecoregions, with the same letter indicating a non-significant difference and different letters indicating a significant difference.

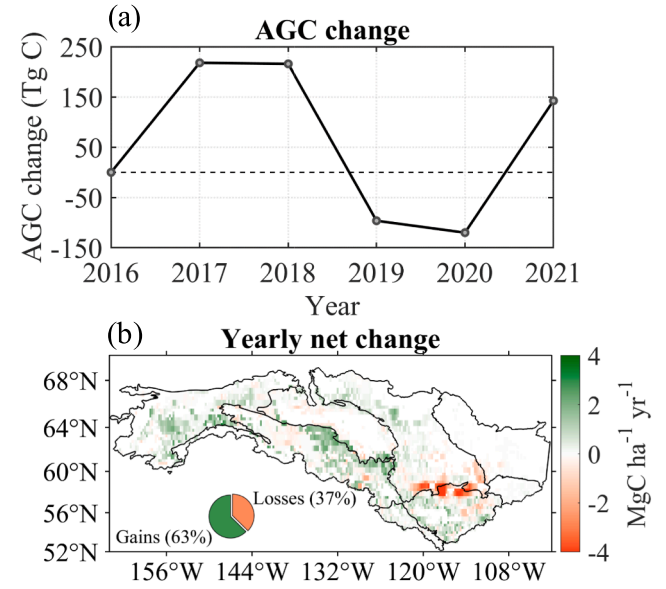


**Fig. 4.** Spatio-temporal variations in annual AGC in the study region. (a) Annual AGC changes in the study region, expressed as the difference from 2016 values. (b) The spatial patterns of yearly AGC net change from 2016 to 2021. The pie graph in (b) represents the percentage of grid cells with gains and losses.

Fig. 5e).

During the study period, there was a considerable decline in AGC in 2019 (-312.21 Tg C) (Fig. 4a). The Boreal cordillera eco-region contributed the largest AGC decline (-159.57 Tg C) (Fig. 5g), followed by the Boreal plain eco-region (-69.72 Tg C) (Fig. 5f), Taiga cordillera eco-region and Alaska boreal interior eco-region were ranked 3rd (-41.27 Tg C) (Fig. 5b) and 4th (-26.87 Tg C) (Fig. 5a) in terms of contribution to this decrease, respectively. This is partly because of the increase in forest cover loss in 2019 (Figure S6). In 2019, Hansen et al. (2013) documented an increase of 199 % in forest loss ($2.8 \times 10^6$ ha) compared with 2018 ($1.4 \times 10^6$ ha) (Figure S6). Forest cover loss in 2019 mainly occurred in the Alaska boreal interior eco-region (Fig. 5a), the Boreal plain eco-region (Fig. 5f) and the Boreal cordillera eco-region (Fig. 5g).

Forests aged 50–70 years old had the maximum net AGC increase (+16.59 Tg C/yr) (Fig. 6a). This increase represented 59 % of the net AGC increase in the study region, suggesting that forests at this stage have the greatest capacity for AGC sequestration. Forests aged 30–50 years old also showed a small AGC increase (+1.99Tg C/yr) (Fig. 6a). Forests older than 70 years showed a decrease in AGC (Fig. 6a), primarily due to an increase in disturbances. The forests aged 10–30 years old was also found to be close to AGC neutrality (Fig. 6a). Regarding tree species, both spruce- and pine forests were the primary contributors to the forest's net AGC increase, representing a net increase of + 9.26 Tg C/yr and + 7.95 Tg C/yr from 2016 to 2021, respectively (Fig. 6b). In contrast, aspen forests were found to experience a net AGC decrease (-4.68 Tg C/yr) (Fig. 6b).

### 4.3. AGC loss resulting from forest cover loss and degradation

We estimated AGC loss resulting from forest cover loss and degradation, respectively (Fig. 7a). Our results showed that 85 % of the total AGC loss was attributed to forest degradation (-162.21 Tg C/yr), with the remaining 15 % attributed to forest cover loss (-28.65 Tg C/yr), indicating that forest degradation contributes significantly more to AGC loss than forest cover loss in North American boreal forests. The major contributors to the total AGC loss from forest cover loss were the Boreal plain eco-region (-9.24 Tg C/yr), the Alaska boreal interior eco-region (-5.53 Tg C/yr), and the Boreal cordillera eco-region (-5.29 Tg C/yr) (Fig. 7a). The collective AGC loss in these three eco-regions constituted 70 % of the total AGC loss attributed to forest cover loss. Additionally, the total AGC loss resulting from degradation was primarily found in the Taiga plain eco-region (-53.72 Tg C/yr), the Boreal plain eco-region (-44.66 Tg C/yr) and the Boreal cordillera eco-region (-39.21 Tg C/yr) (Fig. 7a). In sum, AGC loss in these three eco-regions contributed to 85 % of the total AGC loss resulting from degradation.

The total AGC loss from forest cover loss was subdivided into contributions from stand-replacing fires and other stand-replacing processes (e.g., clear cutting, severe insect outbreaks, and drought). Stand-replacing fires ($5.2 \times 10^6$ ha), covering 44 % of the forest cover loss, contributed 47 % (-13.40 Tg C/yr) of the total AGC loss, with other stand-replacing processes contributed 53 % (-15.25 Tg C/yr) (Fig. 7b). This result suggests that the contribution of stand-replacing fire to AGC loss is comparable to the total AGC loss from all other stand-replacing processes in the study region. The AGC loss from stand-replacing fires was mainly distributed in the Boreal plain eco-region (-3.85 Tg C/yr), the Alaska boreal interior eco-region (-3.09 Tg C/yr) and the Boreal cordillera eco-region (-2.34 Tg C/yr) (Fig. 7b). The Boreal plain eco-region (-5.39 Tg C/yr) also exhibited the largest AGC loss from other stand-replacing processes in the study region, followed by the Boreal cordillera eco-region (-2.95 Tg C/yr) and the Alaska boreal interior eco-region (-2.44 Tg C/yr) (Fig. 7b).

## 5. Discussion

### 5.1. AGC dynamics from 2016 to 2021

Over the period 2016–2021, the average AGC density within the study region was 23.72 Mg C/ha, which is similar to the estimated values using remote sensing method, indicated by 21.36 Mg C/ha for 1984–2014 (Wang et al., 2021); 26.16 Mg C/ha for 2010 (Spawn and Gibbs., 2020), and 27.23 Mg C/ha for 2020 (Santoro, 2023). Note that the AGC density derived from remote sensing methods in the study region (from 21.36 Mg C/ha to 27.23 Mg C/ha), including the AGC density derived from L-VOD (23.72 Mg C/ha), is approximately half lower than the values reported by the forest resource assessment in Canada (45.22 Mg C/ha) (FAO, 2020) and the study based on national forest inventory in Canada (41.3 Mg C/ha) (Sothe et al., 2022). The lower AGC estimates from remote sensing studies (e.g., our study) could be partly explained by the coarser spatial resolution (0.25 degree) of the L-VOD data, which

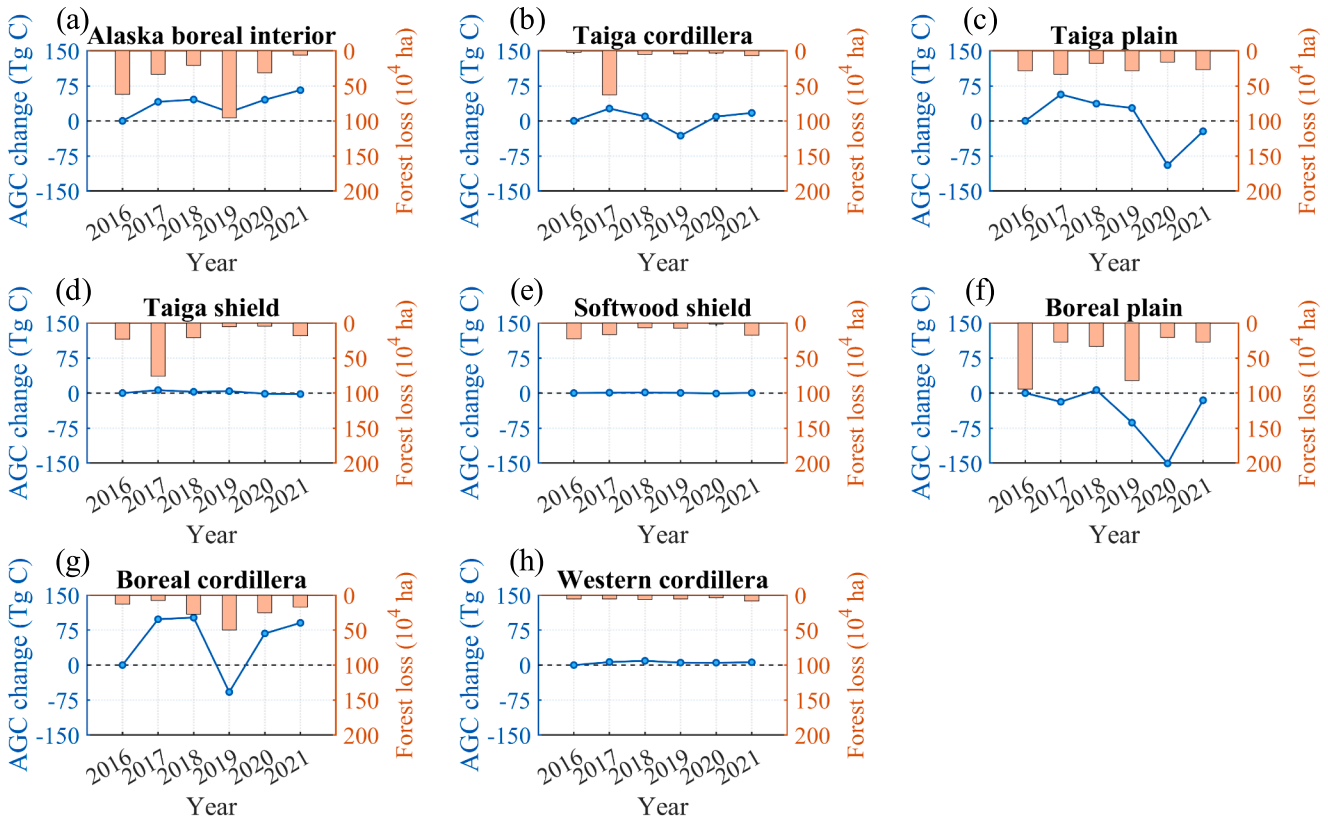


**Fig. 5.** Annual AGC changes in the eight eco-regions, expressed as the difference from 2016 values. (a) Alaska boreal interior eco-region. (b) Taiga cordillera eco-region. (c) Taiga plain eco-region. (d) Taiga shield eco-region. (e) Softwood shield eco-region. (f) Boreal plain eco-region. (g) Boreal cordillera eco-region. (h) Western cordillera eco-region. The yellow bars in (a)-(h) represent the forest loss area. (For interpretation of the references to color in this figure legend, the reader is referred to the web version of this article.)

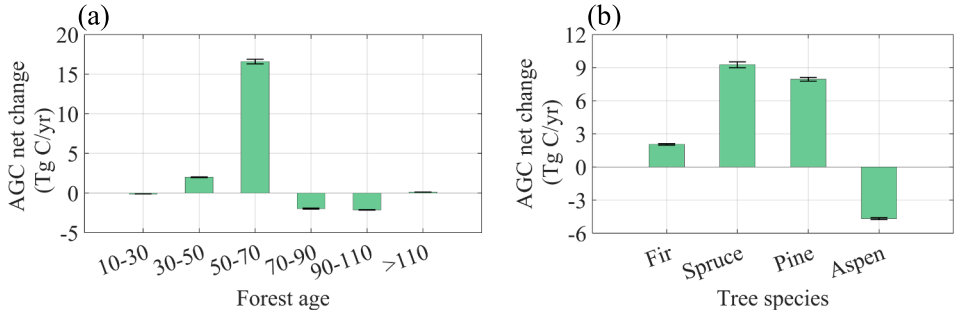


**Fig. 6.** AGC net change for different forest ages (a) and tree species (b). Error bars represent the standard deviation (std).

incorporates non-forest vegetation and potentially results in an underestimation of AGC density. To further analyze the impact of the coarser spatial resolution (0.25 degree) on the underestimation of AGC density, the tree cover data from Hansen et al. (2013) was used to calculate the average tree cover of our study region, which is 49 % (Figure S7). Also, this 49 % tree cover in our study region could be the reason for our AGC estimation being half lower than national forest inventory.

Our results showed that there was a net AGC increase of + 28.49 Tg C/yr in the study region from 2016 to 2021, which contrasts with previous studies reporting AGC declines of about −53.00 Tg C/yr for 2000–2007 (Pan et al., 2011) and −6.42 Tg C/yr for 1993–2012 (Liu et al., 2015). These results partly indicate that North American boreal forests may have transitioned from a state of AGC loss to gain from the late 2000 s to the late 2010 s. It is generally considered that the AGC in North American boreal forests has been declining due to the increasing disturbances in past decades (Kurz et al., 2013). This transition from AGC loss to gain may be due to the high sensitivity of tree growth to the higher temperatures caused by global warming. The increase in AGC from tree growth caused by global warming may have offset the AGC loss from the increase in disturbances in North American boreal forests (Wang et al., 2023). In addition, non-disturbance effects, such as $CO_2$ fertilization and nitrogen (N) deposition can also serve as significant contributors to forest growth in North American boreal forests (Chen et al., 2000).

By comparing our estimated AGC change over 2016–2021 with that of Xu et al. (2021) over 2000–2019, we found that our estimated net AGC change (+28.49 Tg C/yr) is larger than those of Xu et al. (2021) (+10.00 Tg C/yr). The possible explanation for this result could be the saturation observed in the optical remote-sensing data used in the estimation of Xu et al. (2021) over the forest regions, resulting in the high uncertainties in estimates of forest AGC changes (Huete et al., 2002). Relative to optical remote sensing data, L-VOD is less affected by

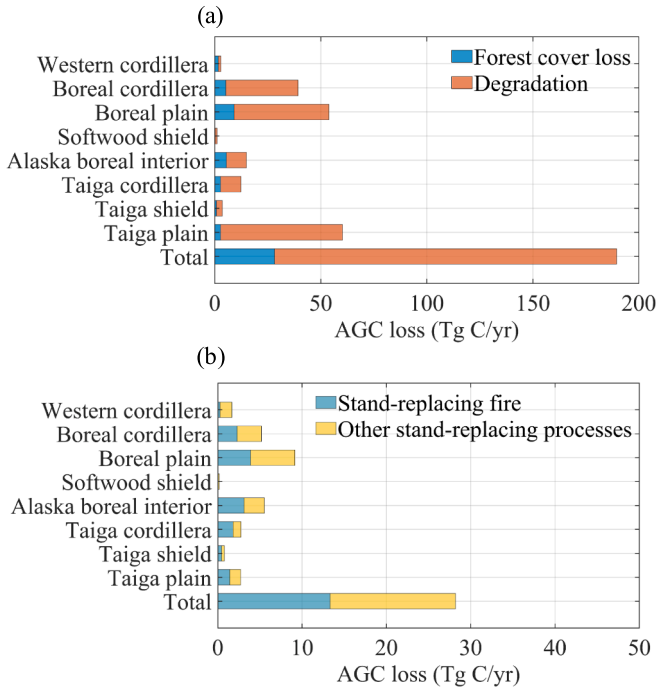


**Fig. 7.** The AGC loss stemming from forest cover loss and degradation. (a) AGC loss stemming from forest cover loss and degradation. (b) AGC loss stemming from stand-replacing fire and other stand-replacing processes.

saturation influence and more correlated with stem-branch AGC (Fan et al., 2019). Thus, L-VOD is likely to provide a more accurate estimation of AGC changes in forests than optical or high-frequency remote sensing datasets.

The total carbon loss across the study region was higher than that estimated by Harris et al. (2021) (–190.86 Tg C/yr vs −123.80 Tg C/yr). The underestimation in Harris et al. (2021) compared to our result can be attributed to the fact that the total carbon loss in Harris et al. (2021) was from stand-replacing disturbances and did not account for the carbon loss from degradation.

### 5.2. Relationships of AGC change with forest age and tree species

Forest age has a direct impact on its ability to absorb carbon from the atmosphere (Besnard et al., 2021). Our results revealed that the net AGC gain peaked in forests aged 50–70 years old, supporting previous finding that forests at this age have the largest carbon sequestration ability (Kolari et al., 2004). This is due to the fact that boreal forests at this stand age (50–70 years old) are typically characterized by closed canopies, and their leaf area index (LAI) generally reaches maximum values (Goulden et al., 2011). Since leaves serve as the primary location for photosynthesis in plants, the photosynthetic capacity of vegetation improves with an increase of LAI (Chen et al., 2019). During this stage (50–70 years old), vegetation respiration is typically weak (Goulden et al., 2011), resulting in a rapid accumulation of vegetation AGC. Our results showed a shift in the net AGC change from an increase to a decline as the forest age exceeded 70 years. This result differs from previous study that suggested old-growth forests uaually function as carbon sinks (Luyssaert et al., 2008). The decline in net AGC change in forests older than 70 years may be attributed to the forest area loss caused by disturbances. By analyzing AGC loss in forests older than 70 years, it was found that AGC loss occurred mainly in the Taiga plain and Boreal plain ecoregion, which shown the greatest forest area loss according to Hansen et al. (2013) (Figure S8). This result suggests that as forests continue to age, they become more vulnerable to disturbances (Kurz et al., 2008b), ultimately resulting in forest AGC loss.

Our results also showed that aspen was a carbon source over the study period. This could be partly due to the weak resistance of aspen to fire (Shinneman et al., 2013). In Canada, crown fires were found to be the predominant forest fire regime (de Groot et al., 2013). Aspen, due to their vulnerability to crown fires, is particularly affected by this type of fire (Shinneman et al., 2013). The thin bark of aspen renders it vulnerable to mixed- or high-severity effects even from low-intensity fires. Furthermore, surviving aspen trees often experience post-fire stress and are highly susceptible to secondary mortality agents (i.e., drought, insect outbreaks and pathogens) (Baker, 2009).

### 5.3. AGC loss caused by forest cover loss and degradation

Our results showed that AGC loss due to forest degradation is 5 times greater than AGC loss due to forest cover loss. This is partly because we attributed degradation to mechanisms not causing forest cover loss. Forest degradation resulting from selective logging (Wang et al., 2021), insect outbreaks (Kurz et al., 2008a), wildfire (Phillips et al., 2022), and drought (Wu and Chen, 2013) can have severe impacts on carbon sinks in North American boreal forests. According to our estimate, the considerable AGC loss stemming from forest degradation should be explicitly factored into carbon budget assessments in North American boreal forests.

We estimated that almost half of the AGC loss due to forest cover loss comes from stand-replacing fire, supporting the primary role of stand-replacing fire in causing carbon loss in this region. Fire stands out as the foremost factor causing stand-replacing disturbance in North American boreal forests, attributed to the vulnerability of tree species to crown fires (Rogers et al., 2015). This type of fire completely burns the aboveground biomass, leading to substantial carbon loss (Zhang et al., 2016). In addition, our results showed that more than half of the AGC loss resulting from forest cover loss comes from other stand-replacing processes (e.g., clear-cutting, severe insect outbreaks and drought), indicating that the role of these processes cannot be ignored in estimating carbon loss in North American boreal forests. In recent years, under the influence of global warming, stand-replacing processes have become increasingly severe (Zhang et al., 2022). The impact of these processes should be emphasized in future estimates of the carbon balance of boreal forests.

### 5.4. Limitations of this study and prospects

The coarse spatial resolution (0.25 degree) of the L-VOD data used in this study limited its capacity to estimate AGC dynamics at a finer scale (Fan et al., 2022). Constrained by the spatial resolution of L-VOD data, both tree species and forest age data were aggregated to 0.25 degree spatial resolution to explore the spatial–temporal variation of AGC across different tree species and forest ages. Yet, the tree species data at 0.25 degree spatial resolution could lead to the loss of some tree species. Thus, the aggregated tree species data only reflects AGC variation for the major tree species. Furthermore, at a spatial resolution of 0.25 degrees, the forest age data could neglect the spatial variability of forest age within a pixel scale, resulting in the underestimation of age in old-growth forests and the overestimation of age in young forests. Thus, future studies should consider finer spatial resolution L-VOD data to accurately estimate AGC and analyze AGC dynamics for finer-scale tree species and forest ages.

The study period from 2016 to 2021 is not long enough to monitor the AGC dynamics over a longer time series. The current retrieval of L-VOD from merged SMOS and SMAP satellite data mainly focuses on improving the accuracy of the algorithm (Li et al., 2022). In the future, studies should concentrate on retrieving longer time series of SMOSS-MAP L-VOD products to estimate the AGC dynamics over a longer time period in North American boreal forests.

This study only concentrated on the live aboveground biomass, and did not address dead wood biomass (e.g., coarse woody debris) and

belowground biomass (e.g., root materials, soils, peatlands, and lakes). A previous study revealed that stand-replacing disturbances or degradation not only cause immediate $CO_2$ release but also increase carbon stocks in dead wood, leading to delayed $CO_2$ emissions from decaying debris and litter (Fan et al., 2022). Furthermore, belowground biomass (e.g., root materials, soils, peatlands, and lakes) accounts for 93 % of the terrestrial carbon pool (Scharlemann et al., 2014), playing a crucial role in determining whether North American boreal forests function as a carbon sink or a carbon source, which is not considered in this study. Thus, future studies that include assessments of live aboveground biomass, dead wood biomass, and belowground biomass will enable a comprehensive assessment of the contribution of North American boreal forests to global carbon dynamics.

## 6. Conclusion

Estimating AGC based on L-VOD provides new insights into how the AGC of western North American boreal forests changes. This study used L-VOD to estimate AGC in western North American boreal forests from 2016 to 2021 and analyzed the spatial–temporal variations of AGC. By combining EPS's Level 2 Ecoregions data, forest age data, and tree species data, we explored AGC changes for different eco-regions, forest age, and tree species. According to the global forest cover loss data, we further estimated the total AGC loss caused by forest cover loss and degradation. Our results showed that the average AGC density in the study region was 23.72 Mg C/ha, and variations observed based on latitude, forest age, eco-region, and tree species. Annual AGC changes indicated that western North American boreal forests experienced a net AGC increase of + 28.49 Tg C/yr from 2016 to 2021, suggesting that these forests acted as a net AGC sink during the study period. Forests at intermediate stand ages (50–70 years old) contributed the most to the AGC increase, followed by forests aged 30–50 years. Yet, forests older than 70 years showed a net AGC decrease. Additionally, both spruce- and pine forests showed a net AGC increase, while aspen forests were found to have a net AGC decrease. Our result also showed that AGC loss due to forest degradation is 5 times greater than AGC loss due to forest cover loss. These results suggest that forest degradation is an important process driving AGC loss in North American boreal forests. Therefore, more attention should be paid to forest degradation in future forest management to protect these forests as a sustainable AGC sink.

## CRediT authorship contribution statement

**Ling Yu:** Writing – review & editing, Writing – original draft, Software, Methodology, Formal analysis, Data curation, Conceptualization. **Lei Fan:** Writing – review & editing, Supervision, Methodology, Funding acquisition, Formal analysis, Conceptualization. **Philippe Ciais:** Writing – review & editing, Conceptualization. **Jingfeng Xiao:** Writing – review & editing, Conceptualization. **Frédéric Frappart:** Writing – review & editing, Conceptualization. **Stephen Sitch:** Writing – review & editing, Conceptualization. **Jingming Chen:** Writing – review & editing, Conceptualization. **Xiangming Xiao:** Writing – review & editing, Conceptualization. **Rasmus Fensholt:** Writing – review & editing. **Zhongbing Chang:** Methodology. **Hongqian Fang:** Methodology. **Xiaojun Li:** Methodology. **Tiangxiang Cui:** Methodology. **Mingguo Ma:** Methodology. **Jean-Pierre Wigneron:** Writing – review & editing.

## Declaration of competing interest

The authors declare that they have no known competing financial interests or personal relationships that could have appeared to influence the work reported in this paper.

## Data availability

The data that support the findings of this study are available at National Tibetan Plateau Data Center, DOI:https://doi.org/10.11888/Terre.tpdc.301109.

## Acknowledgments

This work was supported by National Natural Science Foundation of China (42322103, 42171339).

## Appendix A. Supplementary material

Supplementary data to this article can be found online at https://doi.org/10.1016/j.jag.2024.103729.

## References

Baker, W.L., 2009. Fire ecology in Rocky Mountain Landscapes. Island Press, Washington, D.C.

Besnard, S., Carvalhais, N., Arain, M.A., Black, A., de Bruin, S., Buchmann, N., Cescatti, A., Chen, J., Clevers, J.G.P.W., Desai, A.R., Gough, C.M., Havrankova, K., Herold, M., Hörtnagl, L., Jung, M., Knohl, A., Kruijt, B., Krupkova, L., Law, B.E., Lindroth, A., Noormets, A., Roupsard, O., Steinbrecher, R., Varlagin, A., Vincke, C., Reichstein, M., 2018. Quantifying the effect of forest age in annual net forest carbon balance. Environ. Res. Lett. 13 (12), 124018 https://doi.org/10.1088/1748-9326/aaeaeb.

Besnard, S., Koirala, S., Santoro, M., Weber, U., Nelson, J., Gütter, J., Herault, B., Kassi, J., N'Guessan, A., Neigh, C., Poulter, B., Zhang, T., Carvalhais, N., 2021. Mapping global forest age from forest inventories, biomass and climate data. Earth Syst. Sci. Data 13 (10), 4881–4896. https://doi.org/10.5194/essd-13-4881-2021.

Brandt, M., Wigneron, J.P., Chave, J., Tagesson, T., Penuelas, J., Ciais, P., Rasmussen, K., Tian, F., Mbow, C., Al-Yaari, A., Rodriguez-Fernandez, N., Schurgers, G., Zhang, W., Chang, J., Kerr, Y., Verger, A., Tucker, C., Mialon, A., Rasmussen, L.V., Fan, L., Fensholt, R., 2018a. Satellite passive microwaves reveal recent climate-induced carbon losses in African drylands. Nat. Ecol. Evol. 2 (5), 827–835. https://doi.org/10.1038/s41559-018-0530-6.

Brandt, M., Yue, Y., Wigneron, J.P., Tong, X., Tian, F., Jepsen, M.R., Xiao, X., Verger, A., Mialon, A., Al-Yaari, A., Wang, K., Fensholt, R., 2018b. Satellite-Observed Major Greening and Biomass Increase in South China Karst During Recent Decade. Earth's Future 6 (7), 1017–1028. https://doi.org/10.1029/2018ef000890.

Carreiras, J.M.B., Quegan, S., Le Toan, T., Ho Tong Minh, D., Saatchi, S.S., Carvalhais, N., Reichstein, M., Scipal, K., 2017. Coverage of high biomass forests by the ESA BIOMASS mission under defense restrictions. Remote Sens. Environ. 196, 154-162. http://doi.rog/10.1016/j.rse.2017.05.003.

Chen, J., Chen, W., Liu, J., Cihlar, J., Gray, S., 2000. Annual carbon balance of Canada's forests during 1895–1996. Glob. Biogeochem. Cycle 14 (3), 839–849. https://doi.org/10.1029/1999gb001207.

Chen, J.M., Ju, W., Ciais, P., Viovy, N., Liu, R., Liu, Y., Lu, X., 2019. Vegetation structural change since 1981 significantly enhanced the terrestrial carbon sink. Nat. Commun. 10 (1), 4259. https://doi.org/10.1038/s41467-019-12257-8.

de Groot, W.J., Cantin, A.S., Flannigan, M.D., Soja, A.J., Gowman, L.M., Newbery, A., 2013. A comparison of Canadian and Russian boreal forest fire regimes. For. Ecol. Manage. 294, 23–34. https://doi.org/10.1016/j.foreco.2012.07.033.

Defourny, P., Lamarche, C., Bontemps, S., De Maet, T., Van Bogaert, E., Moreau, I., Brockmann, C., Boettcher, M., Kirches, G., Wevers, J., Santoro, M., Ramoino, F., Arino, O., 2017. Land Cover Climate Change Initiative - Product User Guide v2. Issue 2.0. Available from. http://maps.elie.ucl.ac.be/CCI/viewer/download/ESACCI-LC-Ph2-PUGv2_2.0.pdf.

Dubayah, R., Blair, J.B., Goetz, S., Fatoyinbo, L., Hansen, M., Healey, S., Hofton, M., Hurtt, G., Kellner, J., Luthcke, S., Armston, J., Tang, H., Duncanson, L., Hancock, S., Jantz, P., Marselis, S., Patterson, P.L., Qi, W., Silva, C., 2020. The Global Ecosystem Dynamics Investigation: High-resolution laser ranging of the Earth's forests and topography. Sci. Remote Sens. 1, 100002 https://doi.org/10.1016/j.srs.2020.100002.

Fan, L., Wigneron, J.P., Ciais, P., Chave, J., Brandt, M., Fensholt, R., Saatchi, S.S., Bastos, A., Al-Yaari, A., Hufkens, K., Qin, Y., Xiao, X., Chen, C., Myneni, R.B., Fernandez-Moran, R., Mialon, A., Rodriguez-Fernandez, N.J., Kerr, Y., Tian, F., Penuelas, J., 2019. Satellite-observed pantropical carbon dynamics. Nat. Plants 5 (9), 944–951. https://doi.org/10.1038/s41477-019-0478-9.

Fan, L., Wigneron, J.-P., Ciais, P., Chave, J., Brandt, M., Sitch, S., Yue, C., Bastos, A., Li, X., Qin, Y., Yuan, W., Schepaschenko, D., Mukhortova, L., Li, X., Liu, X., Wang, M., Frappart, F., Xiao, X., Chen, J., Ma, M., Wen, J., Chen, X., Yang, H., van Wees, D., Fensholt, R., 2022. Siberian carbon sink reduced by forest disturbances. Nat. Geosci. 16 (1), 56–62. https://doi.org/10.1038/s41561-022-01087-x.

Fan, L., Xing, Z., Lannoy, G.D., Frappart, F., Peng, J., Zeng, J., Li, X., Yang, K., Zhao, T., Shi, J., Ma, H., Wang, M., Liu, X., Yi, C., Ma, M., Tang, X., Wen, J., Chen, X., Wang, C., Wang, L., Wang, G., Wigneron, J.-P., 2022. Evaluation of satellite and reanalysis estimates of surface and root-zone soil moisture in croplands of Jiangsu Province, China. Remote Sens. Environ. 282 https://doi.org/10.1016/j.rse.2022.113283.

FAO, 2020. Global Forest Resources Assessment 2020: Main report. Rome. http://doi.rog/https://doi.org/10.4060/ca9825en.

Frappart, F., Wigneron, J.-P., Li, X., Liu, X., Al-Yaari, A., Fan, L., Wang, M., Moisy, C., Le Masson, E., Aoulad Lafkih, Z., Vallé, C., Ygorra, B., Baghdadi, N., 2020. Global

Monitoring of the Vegetation Dynamics from the Vegetation Optical Depth (VOD): A Review. Remote Sens. 12 (18), 2915. https://doi.org/10.3390/rs12182915.
Gao, Y., Skutsch, M., Paneque-Gálvez, J., Ghilardi, A., 2020. Remote sensing of forest degradation: a review. Environ. Res. Lett. 15 (10), 103001 https://doi.org/10.1088/1748-9326/abaad7.
Gao, S., Zhou, T., Zhao, X., Wu, D., Li, Z., Wu, H., Du, L., Luo, H., 2016. Age and climate contribution to observed forest carbon sinks in East Asia. Environ. Res. Lett. 11 (3), 034021 https://doi.org/10.1088/1748-9326/11/3/034021.
Gauthier, S., Bernier, P., Kuuluvainen, T., Shvidenko, A.Z., Schepaschenko, D.G., 2015. Boreal forest health and global change. Science 349 (6250), 819–822. https://doi.org/10.1126/science.aaa9092.
Giglio, L., Schroeder, W., Justice, C.O., 2016. The collection 6 MODIS active fire detection algorithm and fire products. Remote Sens. Environ. 178, 31–41. https://doi.org/10.1016/j.rse.2016.02.054.
Goulden, M.L., McMillan, A.M.S., Winston, G.C., Rocha, A.V., Manies, K.L., Harden, J.W., Bond-Lamberty, B.P., 2011. Patterns of NPP, GPP, respiration, and NEP during boreal forest succession. Glob. Change Biol. 17 (2), 855–871. https://doi.org/10.1111/j.1365-2486.2010.02274.x.
Gurney, K.R., Law, R.M., Denning, A.S., Rayner, P.J., Pak, B.C., Baker, D., Bousquet, P., Bruhwiler, L., Chen, Y.-H., Ciais, P., Fung, I.Y., Heimann, M., John, J., Maki, T., Maksyutov, S., Peylin, P., Prather, M., Taguchi, S., 2004. Transcom 3 inversion intercomparison: Model mean results for the estimation of seasonal carbon sources and sinks. Glob. Biogeochem. Cycle 18 (1), GB1010. https://doi.org/10.1029/2003gb002111.
Hansen, M.C., Potapov, P.V., Moore, R., Hancher, M., Turubanova, S.A., Tyukavina, A., Thau, D., Stehman, S.V., Goetz, S.J., Loveland, T.R., Kommareddy, A., Egorov, A., Chini, L., Justice, C.O., Townshend, J.R., 2013. High-resolution global maps of 21st-century forest cover change. Science 342 (6160), 850–853. https://doi.org/10.1126/science.1244693.
Harris, N.L., Brown, S., Hagen, S.C., Saatchi, S.S., Petrova, S., Salas, W., Hansen, M.C., Potapov, P.V., Lotsch, A., 2012. Baseline map of carbon emissions from deforestation in tropical regions. Science 336 (6088), 1573–1576. https://doi.org/10.1126/science.1217962.
Harris, N.L., Gibbs, D.A., Baccini, A., Birdsey, R.A., de Bruin, S., Farina, M., Fatoyinbo, L., Hansen, M.C., Herold, M., Houghton, R.A., Potapov, P.V., Suarez, D.R., Roman-Cuesta, R.M., Saatchi, S.S., Slay, C.M., Turubanova, S.A., Tyukavina, A., 2021. Global maps of twenty-first century forest carbon fluxes. Nat. Clim. Chang. 11 (3), 234–240. https://doi.org/10.1038/s41558-020-00976-6.
Hayes, D.J., Turner, D.P., Stinson, G., McGuire, A.D., Wei, Y., West, T.O., Heath, L.S., Jong, B., McConkey, B.G., Birdsey, R.A., Kurz, W.A., Jacobson, A.R., Huntzinger, D. N., Pan, Y., Post, W.M., Cook, R.B., 2012. Reconciling estimates of the contemporary North American carbon balance among terrestrial biosphere models, atmospheric inversions, and a new approach for estimating net ecosystem exchange from inventory-based data. Glob. Change Biol. 18 (4), 1282–1299. https://doi.org/10.1111/j.1365-2486.2011.02627.x.
Hermosilla, T., Bastyr, A., Coops, N.C., White, J.C., Wulder, M.A., 2022. Mapping the presence and distribution of tree species in Canada's forested ecosystems. Remote Sens. Environ. 282, 113276 https://doi.org/10.1016/j.rse.2022.113276.
Huete, A., Didan, K., Miura, T., Rodriguez, E.P., Gao, X., Ferreira, L.G., 2002. Overview of the radiometric and biophysical performance of the MODIS vegetation indices. Remote Sens. Environ. 83 (1–2), 195–213. https://doi.org/10.1016/S0034-4257(02)00096-2.
Kolari, P., Pumpanen, J., Rannik, Ü., Ilvesniemi, H., Hari, P., Berninger, F., 2004. Carbon balance of different aged Scots pine forests in Southern Finland. Glob. Change Biol. 10 (7), 1106–1119. https://doi.org/10.1111/j.1529-8817.2003.00797.x.
Kurz, W.A., 2010. An ecosystem context for global gross forest cover loss estimates. Proc. Natl. Acad. Sci. U.S.A. 107 (20), 9025–9026. https://doi.org/10.1073/pnas.1004508107.
Kurz, W.A., Dymond, C.C., Stinson, G., Rampley, G.J., Neilson, E.T., Carroll, A.L., Ebata, T., Safranyik, L., 2008a. Mountain pine beetle and forest carbon feedback to climate change. Nature 452 (7190), 987–990. https://doi.org/10.1038/nature06777.
Kurz, W.A., Stinson, G., Rampley, G.J., Dymond, C.C., Neilson, E.T., 2008b. Risk of natural disturbances makes future contribution of Canada's forests to the global carbon cycle highly uncertain. Proc. Natl. Acad. Sci. u. s. a. 105 (5), 1551–1555. https://doi.org/10.1073/pnas.0708133105.
Kurz, W.A., Shaw, C.H., Boisvenue, C., Stinson, G., Metsaranta, J., Leckie, D., Dyk, A., Smyth, C., Neilson, E.T., 2013. Carbon in Canada's boreal forest — A synthesis. Environ. Rev. 21 (4), 260–292. https://doi.org/10.1139/er-2013-0041.
Li, X., Wigneron, J.-P., Frappart, F., Lannoy, G.D., Fan, L., Zhao, T., Gao, L., Tao, S., Ma, H., Peng, Z., Liu, X., Wang, H., Wang, M., Moisy, C., Ciais, P., 2022. The first global soil moisture and vegetation optical depth product retrieved from fused SMOS and SMAP L-band observations. Remote Sens. Environ. 282, 113272 https://doi.org/10.1016/j.rse.2022.113272.
Liu, Y.Y., van Dijk, A.I.J.M., de Jeu, R.A.M., Canadell, J.G., McCabe, M.F., Evans, J.P., Wang, G., 2015. Recent reversal in loss of global terrestrial biomass. Nat. Clim. Chang. 5 (5), 470–474. https://doi.org/10.1038/nclimate2581.
Loboda, T., Hoy, E., Carroll, M., 2019. ABoVE: Study Domain and Standard Reference Grids, Version 2. ORNL DAAC, Oak Ridge, Tennessee, USA, http://doi.rog/https://doi.org/10.3334/ORNLDAAC/1527.
Luyssaert, S., Schulze, E.D., Börner, A., Knohl, A., Hessenmöller, D., Law, B.E., Ciais, P., Grace, J., 2008. Old-growth forests as global carbon sinks. Nature 455 (7210), 213–215. https://doi.org/10.1038/nature07276.
Maltman, J.C., Hermosilla, T., Wulder, M.A., Coops, N.C., White, J.C., 2023. Estimating and mapping forest age across Canada's forested ecosystems. Remote Sens. Environ. 290, 113529 https://doi.org/10.1016/j.rse.2023.113529.
Myers-Smith, I.H., Kerby, J.T., Phoenix, G.K., Bjerke, J.W., Epstein, H.E., Assmann, J.J., John, C., Andreu-Hayles, L., Angers-Blondin, S., Beck, P.S.A., Berner, L.T., Bhatt, U. S., Bjorkman, A.D., Blok, D., Bryn, A., Christiansen, C.T., Cornelissen, J.H.C., Cunliffe, A.M., Elmendorf, S.C., Forbes, B.C., Goetz, S.J., Hollister, R.D., de Jong, R., Loranty, M.M., Macias-Fauria, M., Maseyk, K., Normand, S., Olofsson, J., Parker, T. C., Parmentier, F.-J.-W., Post, E., Schaepman-Strub, G., Stordal, F., Sullivan, P.F., Thomas, H.J.D., Tømmervik, H., Treharne, R., Tweedie, C.E., Walker, D.A., Wilmking, M., Wipf, S., 2020. Complexity revealed in the greening of the Arctic. Nat. Clim. Chang. 10 (2), 106–117. https://doi.org/10.1038/s41558-019-0688-1.
Omernik, J.M., Griffith, G.E., 2014. Ecoregions of the conterminous United States: evolution of a hierarchical spatial framework. Environ. Manage. 54 (6), 1249–1266. https://doi.org/10.1007/s00267-014-0364-1.
Pan, Y., Birdsey, R.A., Fang, J., Houghton, R., Kauppi, P.E., Kurz, W.A., Phillips, O.L., Shvidenko, A., Lewis, S.L., Canadell, J.G., Ciais, P., Jackson, R.B., Pacala, S.W., McGuire, A.D., Piao, S., Rautiainen, A., Sitch, S., Hayes, D., 2011. A Large and Persistent Carbon Sink in the World's Forests. Science 333 (6045), 988–993. https://doi.org/10.1126/science.1201609.
Phillips, C.A., Rogers, B.M., Elder, M., Cooperdock, S., Moubarak, M., Randerson, J.T., Frumhoff, P.C., 2022. Escalating carbon emissions from North American boreal forest wildfires and the climate mitigation potential of fire management. Sci. Adv. 8 (17), eabl7161. https://doi.org/10.1126/sciadv.abl7161.
Pregitzer, K.S., Euskirchen, E.S., 2004. Carbon cycling and storage in world forests: biome patterns related to forest age. Glob. Change Biol. 10 (12), 2052–2077. https://doi.org/10.1111/j.1365-2486.2004.00866.x.
Qin, Y., Xiao, X., Wigneron, J.-P., Ciais, P., Brandt, M., Fan, L., Li, X., Crowell, S., Wu, X., Doughty, R., Zhang, Y., Liu, F., Sitch, S., Moore, B., 2021. Carbon loss from forest degradation exceeds that from deforestation in the Brazilian Amazon. Nat. Clim. Chang. 11 (5), 442–448. https://doi.org/10.1038/s41558-021-01026-5.
Rogers, B.M., Soja, A.J., Goulden, M.L., Randerson, J.T., 2015. Influence of tree species on continental differences in boreal fires and climate feedbacks. Nat. Geosci. 8 (3), 228–234. https://doi.org/10.1038/ngeo2352.
Saatchi, S.S., Harris, N.L., Brown, S., Lefsky, M., Mitchard, E.T.A., Salas, W., Zutta, B.R., Buermann, W., Lewis, S.L., Hagen, S., Petrova, S., White, L., Silman, M., Morel, A., 2011. Benchmark map of forest carbon stocks in tropical regions across three continents. Proc. Natl. Acad. Sci. U.S.A. 108 (24), 9899–9904. https://doi.org/10.1073/pnas.1019576108.
Santoro, M.C., O. , 2023. ESA Biomass Climate Change Initiative (Biomass_cci): Global datasets of forest above-ground biomass for the years 2010, 2017, 2018, 2019 and 2020, v4. NERC EDS Centre for Environmental Data Analysis, 21 April 2023. Available from.https://dx.doi.org/10.5285/af60720c1e404a9e9d2c145d2b2ead4e.
Scharlemann, J.P.W., Tanner, E.V.J., Hiederer, R., Kapos, V., 2014. Global soil carbon: understanding and managing the largest terrestrial carbon pool. Carbon Manag. 5 (1), 81–91. https://doi.org/10.4155/cmt.13.77.
Shendryk, Y., 2022. Fusing GEDI with earth observation data for large area aboveground biomass mapping. Int. J. Appl. Earth Obs. Geoinf. 115, 103108 https://doi.org/10.1016/j.jag.2022.103108.
Shinneman, D.J., Baker, W.L., Rogers, P.C., Kulakowski, D., 2013. Fire regimes of quaking aspen in the Mountain West. For. Ecol. Manage. 299, 22–34. https://doi.org/10.1016/j.foreco.2012.11.032.
Sothe, C., Gonsamo, A., Arabian, J., Kurz, W.A., Finkelstein, S.A., Snider, J., 2022. Large Soil Carbon Storage in Terrestrial Ecosystems of Canada. Glob. Biogeochem. Cycle 36 (2). https://doi.org/10.1029/2021gb007213.
Spawn, S.A., Gibbs., H.K., 2020. Global Aboveground and Belowground Biomass Carbon Density Maps for the Year 2010. ORNL DAAC, Oak Ridge, Tennessee, USA., http://doi.rog/https://doi.org/10.3334/ORNLDAAC/1763.
Stinson, G., Kurz, W.A., Smyth, C.E., Neilson, E.T., Dymond, C.C., Metsaranta, J.M., Boisvenue, C., Rampley, G.J., Li, Q., White, T.M., Blain, D., 2011. An inventory-based analysis of Canada's managed forest carbon dynamics, 1990 to 2008. Glob. Change Biol. 17 (6), 2227–2244. https://doi.org/10.1111/j.1365-2486.2010.02369.x.
Wang, J.A., Baccini, A., Farina, M., Randerson, J.T., Friedl, M.A., 2021. Disturbance suppresses the aboveground carbon sink in North American boreal forests. Nat. Clim. Chang. 11 (5), 435–441. https://doi.org/10.1038/s41558-021-01027-4.
Wang, J., Taylor, A.R., D'Orangeville, L., 2023. Warming-induced tree growth may help offset increasing disturbance across the Canadian boreal forest. Proc. Natl. Acad. Sci. u. s. a. 120 (2) https://doi.org/10.1073/pnas.2212780120.
Wigneron, J.P., Kerr, Y., Waldteufel, P., Saleh, K., Escorihuela, M.J., Richaume, P., Ferrazzoli, P., de Rosnay, P., Gurney, R., Calvet, J.C., Grant, J.P., Guglielmetti, M., Hornbuckle, B., Mätzler, C., Pellarin, T., Schwank, M., 2007. L-band Microwave Emission of the Biosphere (L-MEB) Model: Description and calibration against experimental data sets over crop fields. Remote Sens. Environ. 107 (4), 639–655. https://doi.org/10.1016/j.rse.2006.10.014.
Wu, C., Chen, J.M., 2013. Diverse responses of vegetation production to interannual summer drought in North America. Int. J. Appl. Earth Obs. Geoinf. 21, 1–6. https://doi.org/10.1016/j.jag.2012.08.001.
Xiao, J., Chevallier, F., Gomez, C., Guanter, L., Hicke, J.A., Huete, A.R., Ichii, K., Ni, W., Pang, Y., Rahman, A.F., Sun, G., Yuan, W., Zhang, L., Zhang, X., 2019. Remote sensing of the terrestrial carbon cycle: A review of advances over 50 years. Remote Sens. Environ. 233, 111383 https://doi.org/10.1016/j.rse.2019.111383.
Xu, L., Saatchi, S.S., Yang, Y., Yu, Y., Pongratz, J., Bloom, A.A., Bowman, K., Worden, J., Liu, J., Yin, Y., Domke, G., McRoberts, R.E., Woodall, C., Nabuurs, G.J., de-Miguel, S., Keller, M., Harris, N., Maxwell, S., Schimel, D., 2021. Changes in global terrestrial live biomass over the 21st century. Sci. Adv. 7(27), eabe9829. http://doi.rog/10.1126/sciadv.abe9829.
Yang, H., Ciais, P., Frappart, F., Li, X.J., Brandt, M., Fensholt, R., Fan, L., Saatchi, S., Besnard, S., Deng, Z., Bowring, S., Wigneron, J.P., 2023. Global increase in biomass

carbon stock dominated by growth of northern young forests over past decade. Nat. Geosci. https://doi.org/10.1038/s41561-023-01274-4.

Yu, L., Fan, L., Ciais, P., Sitch, S., Fensholt, R., Xiao, X., Yuan, W., Chen, J., Zhang, Y., Wu, X., Qin, Y., Ma, M., Chang, Z., Wang, M., Yan, K., Song, L., Wigneron, J.-P., 2023. Carbon dynamics of Western North American boreal forests in response to stand-replacing disturbances. Int. J. Appl. Earth Obs. Geoinf. 122, 103410 https://doi.org/10.1016/j.jag.2023.103410.

Zhang, Y., Qin, D., Yuan, W., Jia, B., 2016. Historical trends of forest fires and carbon emissions in China from 1988 to 2012. J. Geophys. Res.-Biogeosci. 121 (9), 2506–2517. https://doi.org/10.1002/2016jg003570.

Zhang, Y., Woodcock, C.E., Chen, S., Wang, J.A., Sulla-Menashe, D., Zuo, Z., Olofsson, P., Wang, Y., Friedl, M.A., 2022. Mapping causal agents of disturbance in boreal and arctic ecosystems of North America using time series of Landsat data. Remote Sens. Environ. 272, 112935 https://doi.org/10.1016/j.rse.2022.112935.

Zhao, Z., Ciais, P., Wigneron, J.-P., Santoro, M., Brandt, M., Kleinschroth, F., L. Lewis, S., Chave, J., Fensholt, R., Laporte, N., Jean Sonwa, D., S. Saatchi, S., Fan, L., Yang, H., Li, X., Wang, M., Zhu, L., Xu, Y., He, J., Li, W., 2023. Central African biomass carbon loss counterbalanced by carbon gains during 2010-2019. One Earth (accept).